

SOME DIAGNOSTIC ASPECTS OF A MODEL RETAINED BAROCLINIC ZONE

W.K. Downey and J.L. McGregor

Australian Numerical Meteorology Research Centre, Melbourne

(Manuscript received December 1978)

ABSTRACT

Diagnostic aspects of a baroclinic zone are examined 9 hours into the integration of a synoptic scale model. The results suggest that such short period integrations can provide a useful base for diagnosing three-dimensional structure and for developing short-term objective forecasting aids.

INTRODUCTION

As well as often being associated with severe weather, baroclinic zones in the atmosphere are important because they are regions in which much of the kinetic energy and vorticity of the atmosphere are concentrated. Synoptic scale numerical models used in the Australian region have received limited attention in relation to:

- (i) how well these features are simulated;
- (ii) how the models might be used diagnostically, for short-term forecasting (0 to 12 hours), or to suggest hypotheses for testing in observational programs.

One reason for the lack of attention is probably the view that the present spatial resolution is too coarse and the physics too crude to expect realistic simulation of such features. While the results presented here will verify that we have a considerable way to go in accurately simulating these features, they do suggest we might make better use of short-term model predictions in ascertaining aspects of three-dimensional structure and indices for objective forecasting aids. Additionally, local budgets of energy and vorticity suggest features that need to be reconciled by future studies in both the real world and model environments.

A CASE STUDY

The situation of 9-10 November 1977 (Fig. 1) is a useful illustration of a sharp baroclinic zone affecting southeastern Australia. On this occasion severe wind damage occurred at many locations; Adelaide, Mildura, Griffith, and Canberra being some of the major cities so affected in the 24-hour period to 2300 GMT 9 November 1977. It is clear from Figs 1(c) and (e) that the 'wave cyclone' in northwest Victoria at 0900 GMT 9 November was not captured in the Australian Region Primitive Equations (ARPE) model and that this would have some bearing on forecasts of the broadscale wind setting. However, two factors should be kept in mind:

- (i) mesoscale analysis (Downey and Streten 1978) suggests that in this case the severe wind damage is primarily attributable to the interaction of deep convection (thunderstorms) and the background baroclinicity (shear);

- (ii) the location of the broadscale trough and the jet structure at 500 mb (Figs 1(d), (f)) are reasonably well captured in the model.

On this basis we address ourselves to the question of what additional diagnostic information we might extract from a limited integration of the model and how that information might be used in the development of objective forecasting aids.

The ARPE model

To appreciate the model results that will subsequently be presented, it is necessary to note some of the features of the model. These are outlined in McGregor et al. (1978) and are comprehensively summarised in Fig. 2. The points of particular interest to the present study are (i) the limited horizontal (250 km) and vertical (6 levels equally spaced in σ) resolution and (ii) the absence of any physics that would incorporate diurnal heating of the earth's surface and sensible heat exchange with the atmosphere. Despite these deficiencies the baroclinic zone is retained in some detail in the model integration. A period of 9 hours into the integration has been selected for diagnostic purposes for the following reasons:

- (i) the model is initialised in such a way that the wind field is substantially non-divergent at $t = 0$. It therefore takes some time for the three-dimensional structure to become established;
- (ii) we do not want to go so far into the integration that the error growth due to data and model deficiencies become unreasonably dominant.

ALTERNATIVE MODEL OUTPUT

The major component of current prognosis output remains the MSL pressure field. It is an extremely useful tool in terms of inferring the broadscale surface wind flow, gross temperature tendencies, and to a lesser degree the likely cloud/weather conditions. However, given that there are a number of parameters other than pressure and geopotential height that can be calculated within the model framework, one must ask if some of these might prove to be useful objective aids for some of the shorter term forecast problems. Figure 3 illustrates some of the field quantities that might be relevant in this regard.

The low level ($k = 6$, $p \sim 900$ mb) baroclinic zone and an attendant band of convergence are shown in Fig. 3(a). As might be expected the vertical motion field at level 4 (Fig. 3(b)) tends to be a direct reflection of the lower level convergence field. The RH at level 4 (Fig 3(c)) similarly reflects line structure that is in reasonable agreement with the observed location of frontal cloud from a DMSP satellite.

A point of interest in relation to the orientation of the line structure in these model fields is their rotation clockwise by some 30 to 40 degrees with respect to the baroclinic zone. This feature is noted in some satellite observed cloud bands, and is in agreement with the vertical motion fields expected in the vicinity of entrance/exit regions of jet streaks, based on quasi-geostrophic theory.

Since the severe wind damage associated with this type of situation is believed to result from convection in a strongly sheared environment (Downey and Stretten 1978) a parameter such as the Richardson number (R.), which incorporates the effects of shear and static stability, could be a useful index.

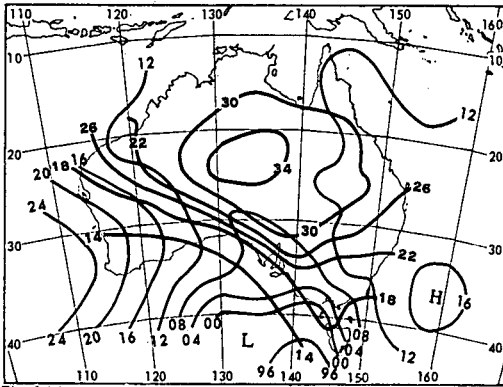


Fig. 1 (a)

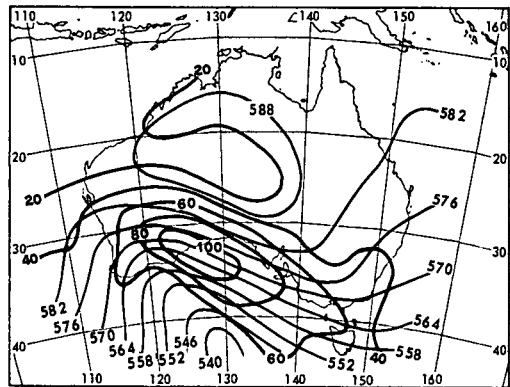


Fig. 1 (b)

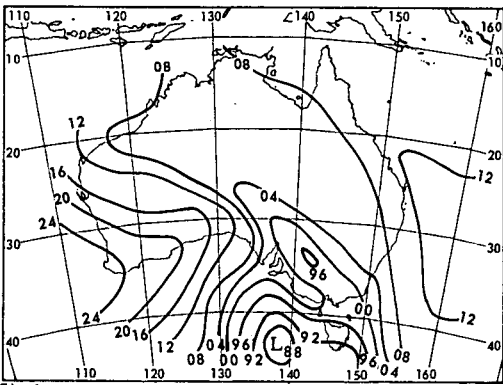


Fig. 1 (c)

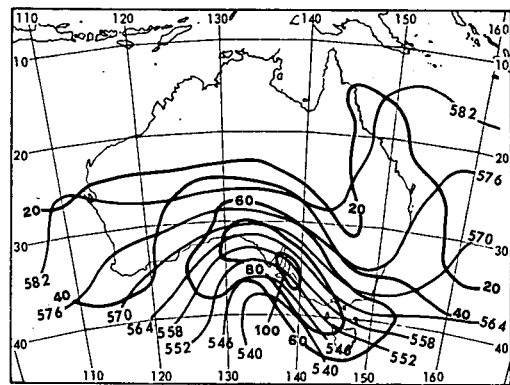


Fig. 1 (d)

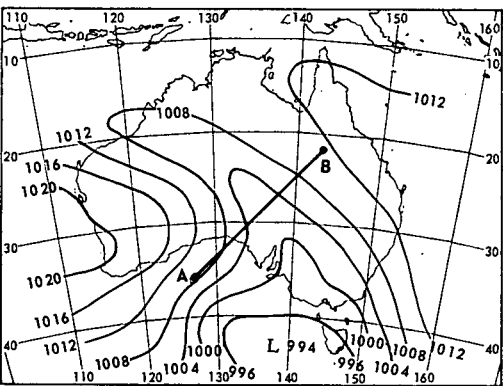


Fig. 1 (e)

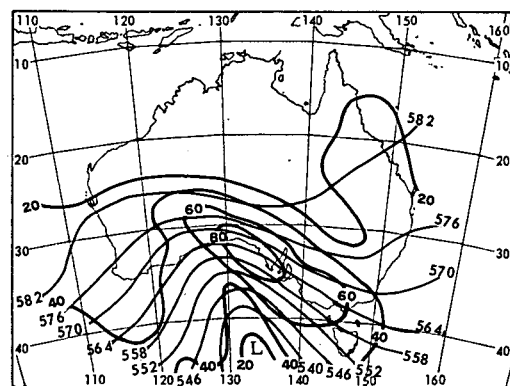


Fig. 1 (f)

Fig. 1 (a) Mean sea level pressure (mb) and surface temperature (thick lines ...°C) for 0000 GMT 9 November 1977.
 (b) 500 mb contours (decametres) and isotachs (thick lines ... kn) for 0000 GMT 9 November 1977.
 (c) Mean sea level pressure (mb) analysis for 0900 GMT 9 November 1977.
 (d) 500 mb contour - isotach analyses for 1200 GMT 9 November 1977.
 (e) Forecast MSL pressure (mb) 0900 GMT 9 November 1977. A-B denotes the line used in subsequent cross-sections.
 (f) Forecast 500 mb contours and isotachs for 0900 GMT 9 November 1977.

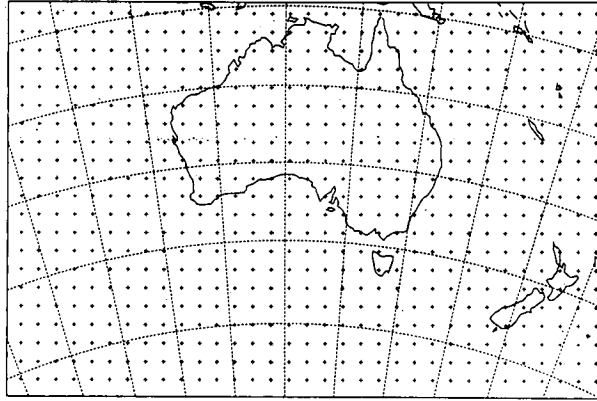


Fig. 2 (a)

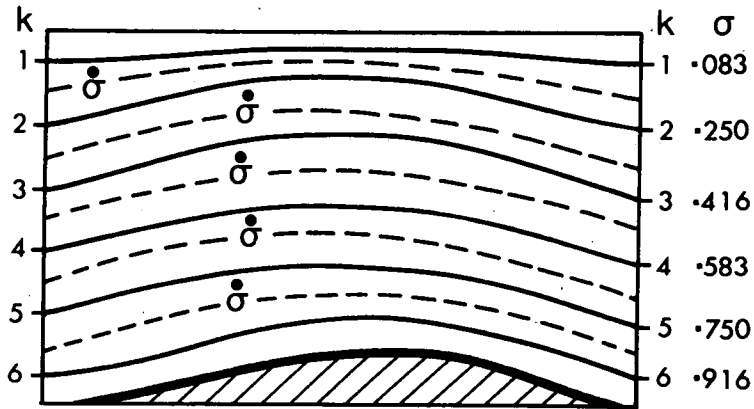


Fig. 2 (b)

Independent variables x, y, σ, t
Time-dependent variables u, v, σ, T, p_*, q
Historical variables u, v, T, p_*, q
Grid-square on Lambert conformal projection: u, v staggered
Mesh width 250 km
Time integration. Semi-implicit; 36 min timestep
Friction, bulk aerodynamic drag at level 6
 C_D land = 0.004 ocean = 0.001. Some vertical diffusion
Sensible heat } only in terms of convective parameterisation
Latent heat }
Radiation is not included
Smoothing/filtering/treatment at lateral boundaries
 (i) Time smoothing $f_{\tau} = 0.1 f_{\tau+1} + 0.8 f_{\tau} + 0.1 f_{\tau-1}$
 (ii) Spatial smoothing at all boundaries.

Fig. 2 (c)

Fig. 2 Some details of the Australian Region Primitive Equation Model

- (a) The analysis-forecast domain and the horizontal grid spacing
- (b) The vertical structure
- (c) Physical specifications

In Fig. 3(d) the inverse of R_i for level $4\frac{1}{2}$ is displayed¹. The northwest-southeast orientation of this field reflects the substantial contribution of the shear term along the baroclinic zone. In the next section we shall examine some of these features in a vertical section normal to the baroclinic zone.

Cross-sections

Figure 4 shows the distribution of isentropes (θ) and isotachs in a plane approximately normal to the baroclinic zone (i.e. along AB in Fig. 3). Features of note are the poleward slope to the baroclinic zone (stippled²) and a region of reduced static stability ($\frac{\partial\theta}{\partial\sigma}$) on the warm side of the zone. The wind component shown in Fig. 4(a) is that normal to the section and reveals the strong vertical shear in the baroclinic zone as well as the general horizontal shear associated with the jet. Values of R_i^{-1} (Fig. 4(c)) indicate maximum values along the leading edge of the baroclinic zone and in the lower and middle troposphere. The distribution of potential vorticity is shown only to indicate the 'extrusion' of stratospheric air within the baroclinic zone (Danielsen 1964). Horizontal divergence and vertical motion ($\frac{d\sigma}{dt}$) are shown in Fig. 4(b). Strong low-level convergence and ascent occur at the leading edge of the surface baroclinic zone with strong mid-tropospheric subsidence on the cyclonic side of the jet. The latter feature is consistent with the prevailing flow into the 'right rear' entrance region of the jet streak.

Budget aspects

Since a baroclinic zone is attended by concentrations of vorticity and kinetic energy it is of some interest to examine the way in which the various sources/sinks and transports affect the respective budgets of these properties. In undertaking such an exercise there is no particular geometry that suggests itself as being uniquely suitable as a budget volume. For the purposes of the present study a square domain is selected with the line A-B (Fig. 3(a)) forming one of the diagonals. This facilitates retention of features either side of the baroclinic zone, but the influence of such features diminishes with their distance therefrom.

The budget framework

Following Johnson and Downey (1975) the generalised budget equation for a stationary budget volume can be written:

$$\frac{\partial}{\partial t} B_{\sigma_1, \sigma_2} = \int_{\sigma_1}^{\sigma_2} \int_A \frac{p_*}{g} \frac{db}{dt} dAd\sigma + \int_{\sigma_1}^{\sigma_2} \oint \frac{p_*}{g} b U_n dLd\sigma + \int_{\sigma_1}^{\sigma_2} \int_A \frac{p_*}{g} \frac{\partial}{\partial \sigma} (b\sigma) dAd\sigma$$

SOURCES/SINKS
LATERAL TRANSPORT
VERTICAL TRANSPORT

¹ $R_i^{-1} = \frac{\partial v}{\partial z}^2 / \left(\frac{g}{\theta}\right) \left(\frac{\partial \theta}{\partial z}\right)$ is used so that large values correspond to the regions of most interest. In general R_i^{-1} could approach infinity, however in the convective adjustment scheme of the model a lower limit of $\frac{\partial \theta}{\partial \sigma} = 0.6 \text{ K.atm}^{-1}$ is prescribed.

² The stippled area is a subjective interpretation of the location of the baroclinic zone and the tropopause based on considerations of the distribution of shear, static stability, horizontal temperature gradients, and potential vorticity.

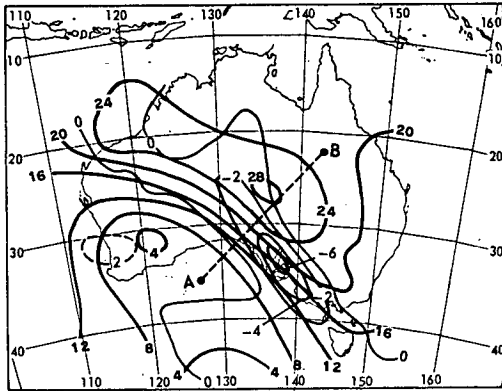


Fig. 3(a)

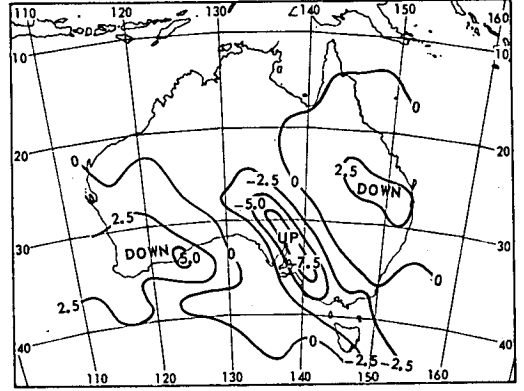


Fig. 3(b)

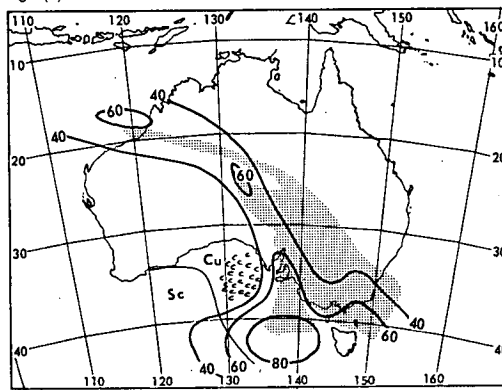


Fig. 3(c)

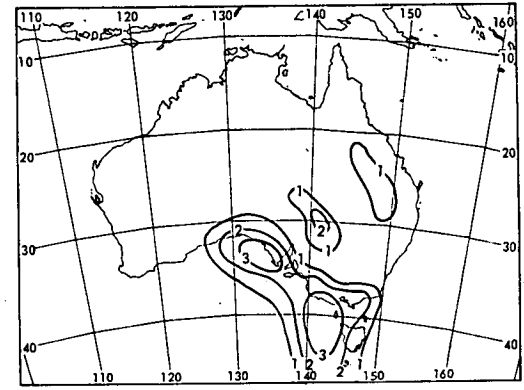


Fig. 3(d)

Fig. 3 Forecast values for 0900 GMT 9 November 1977 of:

- (a) temperature ($^{\circ}\text{C}$) at level 6 (≈ 920 mb) and divergence ($\times 10^{-5} \text{ s}^{-1}$.. thin lines);
- (b) $\frac{d\sigma}{dt}$ ($\times 10^{-6} \text{ s}^{-1}$) at level 4 (≈ 580 mb);
- (c) relative humidity (%) at level 4 (the observed cloud analysis (stippling) is based on DMSP imagery at 1400 GMT);
- (d) R_i^{-1} ($\times 10^{-1}$) at level $4\frac{1}{2}$ (~ 660 mb).

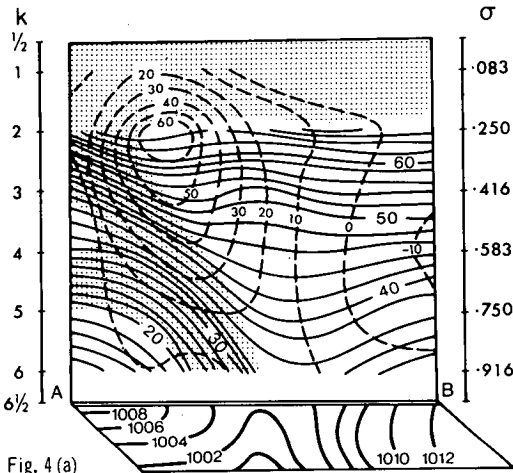


Fig. 4 (a)

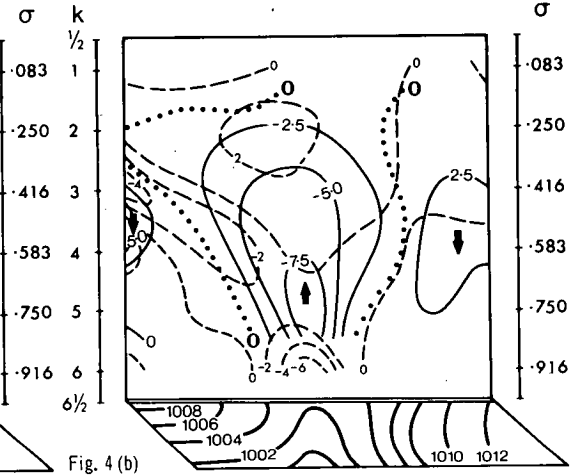


Fig. 4 (b)

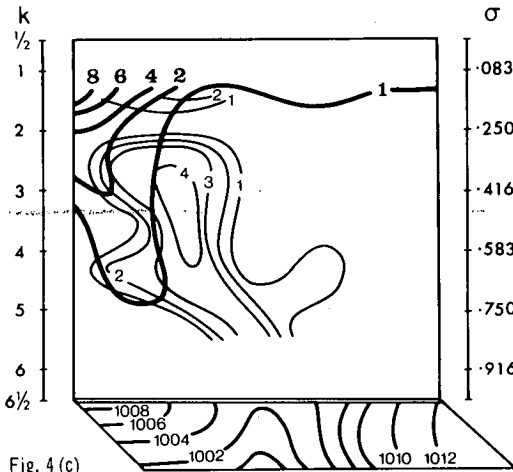


Fig. 4 (c)

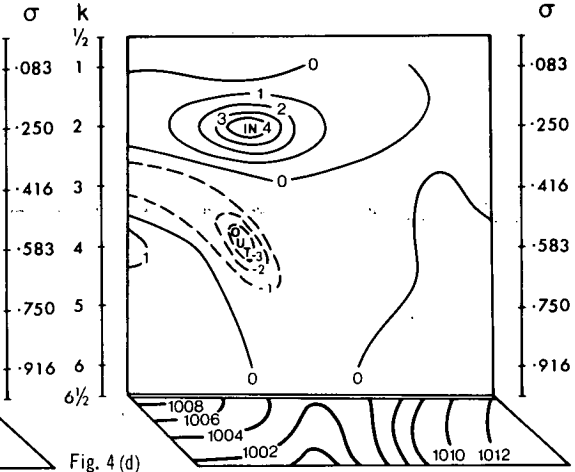


Fig. 4 (d)

Fig. 4 Cross-sections of:

- (a) potential temperature ($^{\circ}\text{C}$) and isotachs (ms^{-1} .. dashed lines);
- (b) divergence ($\times 10^{-5} \text{s}^{-1}$) and $\frac{d\sigma}{dt}$ ($\times 10^{-6} \text{s}^{-1}$.. solid lines);
- (c) R_i^{-1} ($\times 10^{-1}$) and potential vorticity ($\times 10^{-8} \text{K} \cdot \text{s}^{-1} \cdot \text{mb}^{-1}$.. heavy lines);
- (d) vertical transport of kinetic energy ($\times 10^2 \text{ watt} \cdot \text{m}^{-2} \text{atm}^{-1}$);

based on model output for 0900 GMT, 9 November 1977.

where

$$B_{\sigma_1, \sigma_2} = \int_{\sigma_1}^{\sigma_2} \int_A \frac{p_*}{g} b \, dA d\sigma; \quad p_* = \text{surface pressure}; \quad A = \text{area}; \quad L = \text{lateral bound-}$$

ary; U_n = velocity normal to the lateral boundary; b = budget quantity (per unit mass). For the mass budget $b = 1$; $\frac{db}{dt} = 0$. For the kinetic energy budget $b = \underline{u} \cdot \underline{u}/2$; $\frac{db}{dt} = -\underline{U} \cdot \underline{\nabla} \phi + \underline{U} \cdot \underline{F}$, where ϕ = geopotential height; \underline{F} = frictional force. For the vorticity budget $b = [(\underline{k} \cdot \underline{\nabla} \times \underline{U}) + f] = \zeta + f$ and

$$\frac{db}{dt} = -(\zeta + f) \cdot \underline{\nabla} \phi - \underline{u} \cdot \underline{k} \cdot \underline{\nabla} \sigma \times \frac{\partial \underline{u}}{\partial \sigma} + \underline{k} \cdot \underline{\nabla} \times \underline{F}$$

(STRETCHING) (TIPPING) (FRICTION)

(Note: the solenoid term is small and is neglected.)

Mass budget

The profile of lateral mass transport for the defined budget volume is shown in Fig. 5(a). It is similar to that observed for the larger domain of an extratropical cyclone (Downey and Johnson 1978). The low level mass convergence is closely balanced by upper-level divergence in accordance with a slowly varying surface pressure tendency. Note however that while the convergence is sustained over several levels ($k = 3$ to 6) the compensation virtually occurs entirely at level 2.

Kinetic energy budget

The vertical profiles of the terms in the kinetic energy budget are shown in Fig. 5(b). Their net effect is an increase in kinetic energy at the main jet level ($k = 2, 3$) and a decrease above and below. The increase at $k = 2, 3$ results from an excess of vertical transport (from below) and local generation, over the lateral export of kinetic energy. The decrease above level 2 is the result of negative generation while the decrease at level 4 is due to vertical export exceeding lateral import and local generation. In the boundary layer ($k = 5, 6$) generation slightly exceeds frictional dissipation and vertical export.

An interesting aspect of the budget in the vicinity of the jet streak is the substantial role of the vertical transport of kinetic energy. Some observational studies on both the cyclone scale (e.g. Chen and Bosart 1977, Vincent and Chang 1975) and the mesoscale (e.g. Kung and Tsui 1975) have suggested that the vertical transport of k.e. can adopt a role comparable to generation and lateral transport with values approaching 50 to 100 watt $m^{-2} atm^{-1}$. These observational results have been used to make inferences regarding 'upscale' energy cascades. While the model results cannot comment directly on the cascade question (such effects would have to be explicitly formulated in the model) the general confirmation of large vertical transports in the vicinity of a jet streak is of some relevance to this general area of study.

The distribution of the vertical transport in the cross-section plane utilised earlier is shown in Fig. 4(d). In this case kinetic energy is being transported vertically into the jet from the leading edge of the baroclinic zone below.

Vorticity budget

Within the stationary budget volume it is clear from Fig. 5(c) that the vorticity is increasing at all levels. The dominant influence in producing this result

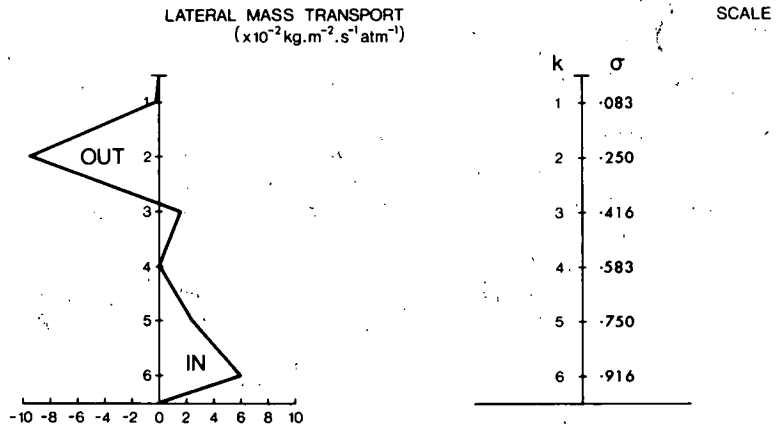


Fig. 5 (a)

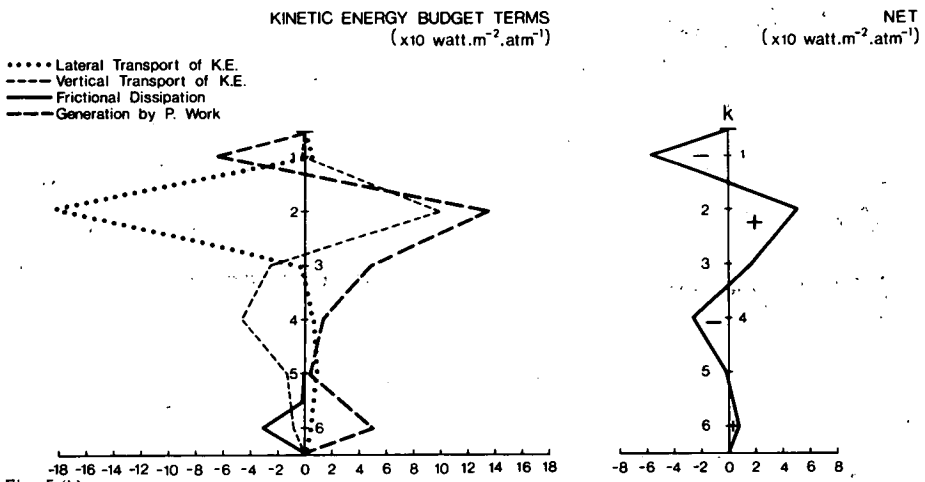


Fig. 5 (b)

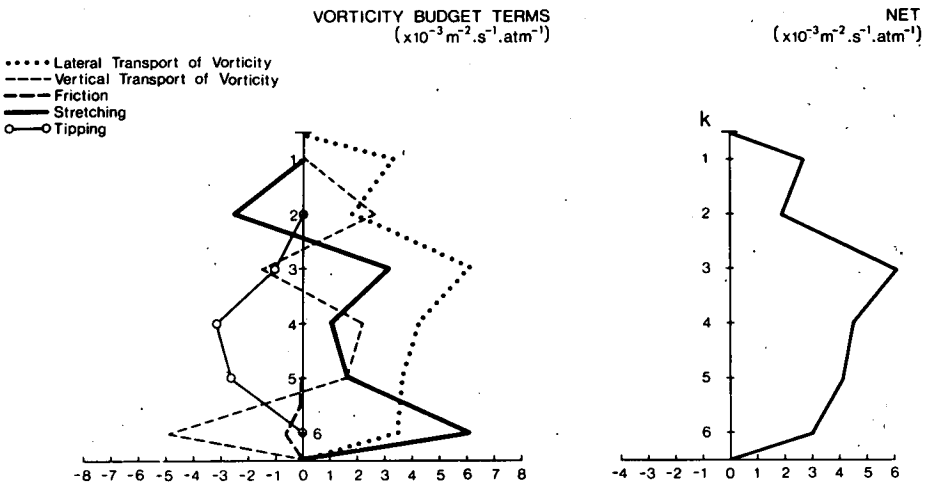


Fig. 5 (c)

Fig. 5 Budget profiles for 0900 GMT 9 November 1977.

appears to be the lateral transport term since, while tipping, vertical transport, and stretching are of comparable magnitude, these latter terms tend to compensate each other. (Note, however, that the way in which they compensate is not the same at all levels e.g. compare levels 5 and 3 in Fig. 5(c).)

Other features of note in the vertical profiles are:

- (i) large net sink (i.e. after vertical integration) of vorticity associated with the tipping term and the net source of vorticity due to stretching;
- (ii) the 'zig-zag' structure of the vertical transport term and its form in relation to the stretching term. This reflects a substantial role for vertical vorticity advection, the reasoning being as follows.

The vertical transport term is given by

$$\begin{aligned} \text{V.T.} &= \frac{\partial}{\partial \sigma} [(\zeta+f) \dot{\sigma}] \\ &= (\zeta+f) \frac{\partial \dot{\sigma}}{\partial \sigma} + \dot{\sigma} \frac{\partial \zeta}{\partial \sigma}. \end{aligned}$$

Now to a large extent $(\zeta+f) \frac{\partial \dot{\sigma}}{\partial \sigma}$ represents the negative of the stretching term - $(\zeta+f) \nabla_{\sigma} \cdot \mathbf{V}$ and so in regions where $\frac{\partial \zeta}{\partial \sigma}$ is small one would expect the vertical transport and stretching terms to compensate. In Fig. 5(c) one sees a degree of compensation above $k = 2$ and below $k = 5$; however, the intervening layers are characterised by strong vertical advection as a result of the vorticity gradients through the baroclinic zone. The reason for near compensation of [stretching + tipping + vertical transport] is unclear and requires further study.

SUMMARY AND CONCLUSIONS

In this paper we have diagnosed a number of features associated with a model retained baroclinic zone. The diagnostics are undertaken some 9 hours into the integration of a synoptic scale model when the four-dimensional structure has had some chance to become established and where we might expect error growth due to inadequate physics and resolution to be reasonably bounded. We suggest that such short period integrations have the potential to provide a useful base for (i) diagnosing three-dimensional structure and the role of various terms in the local energy and vorticity budgets and (ii) developing short term objective forecasting aids, e.g. parameters such as $R_i^{-1} |\nabla \cdot \mathbf{V}|_{k=6}$ may be useful in multiple regression techniques for severe wind damage.

REFERENCES

- Chen, T.J.G. and Bosart, L.F. 1977. Quasi-Lagrangian kinetic energy budgets of composite cyclone-anticyclone couplets. *J. Atmos. Sci.*, 34, 451-65.
- Danielsen, E.F. 1964. *Report on Project Springfield*. (Defence Atomic Support Agency: Washington D.C.) 99p.
- Downey, W.K. and Johnson, D.R. 1978. The mass, absolute angular momentum and kinetic energy budgets of a model generated extratropical cyclone. *Mon. Weath. Rev.*, 106, 469-81.
- Downey, W.K. and Stretten, N.A. 1978. The use of temporally frequent high resolution satellite imagery for mesoscale analysis and trend forecasting. *Proceedings of AIRMET Conference Canberra*; Roy. Met. Soc. Australian Branch.

Johnson, D.R. and Downey, W.K. 1975. Azimuthally averaged transport and budget equations for storms: quasi Lagrangian diagnostic. *Mon. Weath. Rev.*, 103, 967-79.

Kung, E.C. and Tsui, T.L. 1975. Subsynoptic-scale kinetic energy balance in the storm area. *J. Atmos. Sci.*, 32, 729-40.

McGregor, J.L., Leslie, L.M. and Gauntlett, D.J. 1978. The ANMRC limited-area model: consolidated formulation and operational results. *Mon. Weath. Rev.*, 106, 427-38.

Vincent, D.G. and Chang, L.N. 1975. Kinetic energy budgets of moving systems: case studies for an extratropical cyclone and hurricane Celia, 1970. *Tellus*, 27, 215-33.

